S.T. Yau High School Science Award (Asia)

Research Report

The Team

Registration Number: Chem-005

Name of team member: LEUNG Long Hei Ziv
School: The Chinese Foundation Secondary School
Country: HKSAR, China

Name of supervising teacher: HO Chun Man
School: The Chinese Foundation Secondary School
Country: HKSAR, China

Title of Research Report

Wearable Textile-based Direct Urea Fuel Cell

Wearable Textile-based Direct Urea Fuel Cell

LEUNG Long Hei Ziv

Abstract

There is currently an interest in developing wearable energy harvesting devices as the booming of various microsystem applications, such as health care, medical rehabilitation, athletic training, and outdoor equipment[1, 2]. Conventionally, wearable devices are mainly powered by batteries and thus have a limited working time period. Energy renewal or battery recharge for the devices is unavoidable[3, 4]. To address this issue, the self-powered scheme, in which the device's power is supplied by an attached wearable energy harvester, is increasingly attracting attention[5, 6, 7].

Our wearable energy harvesting device, direct urea fuel cell (DUFC), aims at generating electricity by using urea in sweat. An NiZnCu alloy-based orderly aligned nanorod array anode is integrated with a CQD-Carbon electrode and assembled on a flexible textile or hydrogel substrate. Based on the oxidation of urea over the NiZnCu alloy-based catalyst and reduction of oxygen at air electrode, a direct urea fuel cell is formed to generate stable amount of electric energy. $Cu(OH)_2$ aligned nanorods were firstly grown on the Cu-foam by immersing Cu-foam in alkaline $(NH_4)_2S_2O_8$ solution, followed by chemical reduction to give Cu nanorod array. Cu nanorod array was then electroplated with Zn in alkaline $Zn(OH)_4^{2-}$ and doped with Ni in $Ni(OH)_4^{2-}$ solution, followed by annealing. Nanostructured morphology and chemical composition were examined and confirmed by SEM and EDX analysis.

The wearable DUFC is fabricated and assembled via a combination of lithographically-patterned silver-load circuit framework together with anode and cathode array arranged in an island-bridge configuration[8]. The effects of temperature, urea concentration and pH conditions on DUFC performance were investigated. Our model exhibits an open circuit voltage of 0.917 V, power density of nearly 15.2 mW cm^{-2} with current density of 30.6 mA cm^{-2}, capacity of 47 mAh and energy capacity of 20 mWh when 0.3 M urea was used as fuel, air as oxidant at 298 K, which open up the possibility of developing the real-life application of a soft, flexible wearable direct urea fuel cell.

Keywords: Wearable device, flexible fuel cell, direct urea fuel cell

Acknowledgement

Appreciation goes to the Guangzhou Yahong Testing Technology Company for their technical support on the XRD Analysis and EDX/elemental mapping analysis.

Table of Contents

Section I Introduction

There is currently an interest in developing wearable energy harvesting devices as the booming of various microsystem applications, such as health care, medical rehabilitation, athletic training, and outdoor equipment[1, 2]. Conventionally, wearable devices are mainly powered by batteries and thus have a limited working time period. Energy renewal or battery recharge for the devices is unavoidable[3, 4]. To address this issue, the self-powered scheme, in which the device's power is supplied by an attached wearable energy harvester, is increasingly attracting attention[5, 6, 7]. Our wearable energy harvesting device, direct urea fuel cell (DUFC), aims at generating electricity by using urea in sweat.

Biofuel cells convert biochemical energy present in biofluids to electrical power through redox reactions that use enzymes and/or noble metal-based catalyst. The power density largely depends on the availability of chemical sources in biofluids and the electron transfer efficiency between chemical and electrodes[8]. Biofuel cells require intimate and conformal contact with the human body in order to maintain continuous and efficient power extraction from biofluids such as sweat. Urea in sweat is a promising fuel as it has higher energy density then compressed or liquid hydrogen which make urea a potential energy carrier (Figure 1.1)[9].

Compound	Density / g cm^{-3}	Gravimetric H_2 density / % H_2	Volumetric H_2 density / kg H_2 dm^{-3}	Energy density / MJ dm^{-3}
Gaseous H_2	8.988×10^{-5}	100	8.988×10^{-5}	0.01079
Compressed H_2	0.039	100	0.039	5.6
Liquid H_2	0.071	100	0.071	10.1
Aqueous NH_3 (28%)	0.747	2.4	0.13	12.6
Liquid NH_3	0.747	17.6	0.13	12.6
Urea	1.335	10.07	0.134	16.9

Figure 1.1 Comparison of energy density of different materials

Direct urea fuel cells, DUFC, would be an efficient method of generating power from urea in sweat. Potentially, DUFC can use sweat (or urine) as the fuel. In this case, urea, a product of human and animal excretion, is not a waste, but an energy source. The operating mechanism of a DUFC using an alkaline membrane electrolyte is describe below:

Cathode: $O_2 + 2H_2O + 4e^- \rightleftharpoons 4OH^-$ $E^e = +0.40$ V

Anode: $CO(NH_2)_2 + 6OH^- \rightleftharpoons N_2 + CO_2 + 5H_2O + 6e^-$ $E^e = -0.75$ V

Overall: $2CO(NH_2)_2 + 3O_2 \rightleftharpoons 2N_2 + 2CO_2 + 4H_2O$ $E^e_{cell} = +1.15$ V

The theoretical open circuit voltage (V_{OC}) of DUFC is 1.15 V at room temperature, slightly lower than the 1.23 V for a hydrogen-oxygen fuel cell. However, the theoretical efficiency of a DUFC is 103% at room temperature which is about 20% higher than that of hydrogen-oxygen fuel cell (83% at room temperature)[9].

Conventional DUFC always involves the usage of precious metals such as Pt as the catalyst. Owing to limited resource and production cost of these materials, it does not meet the requirement of "green DUFC" for next generation power devices. Therefore, development of DUFC using renewable biomaterials is an unarguable topic in scientific research. The objective of this project is to find an environmentally benign alternative for building various key components of flexible wearable DUFC structures. The proposed green alternatives for each component are present in Figure 1.2.

	Conventional	Our model
Fuel	Lactic acid	Urea in sweat
Oxidant	Oxygen in air	
Catalyst	Anode: Enzyme, lactate Cathode: Pt	Anode: Ni doped Cu-Zn alloy Cathode: Pt or CQD
Substrate	Bulky design	Flexible wearable DUFC

Figure 1.2 Alternative renewable materials for DUFC fabrication

A simple and high efficiency carbon-based catalyst can be used to replace expensive Pt catalyst to catalyze the oxygen reduction and oxygen evolution reaction occurred at cathode. Nanostructured carbon-based particles are usually prepared from derivation of various biomass such as carbonization of eggplant, coconut shell, cellulose, or hydrothermal treatment of carbohydrates like glucose, sucrose or gelatin. In this project, carbon quantum dots (CQDs) were prepared from carbonization of gelatin. The as-prepared CQDs are generally small carbon nanoparticle with the size less than 10 nm. The carbon particles act as the bifunctional catalysts for the oxygen reduction and the oxygen evolution reaction occurred in the air electrode.

In this report, we explore designs of fully operational wearable prototype DUFC composed entirely of highly efficient and stable alloy-based catalyst for anode and CQDs for the cathode. The presented materials are all originated from simple and biodegradable source compounds, which decrease the environmental impact of their manufacture.

Section II Preparation of Cu/Zn Alloy-based Orderly Aligned Nanorod Array Electrode

2.1 Introduction

The operating mechanism of a direct urea fuel cell (DUFC) using an pH-buffered electrolyte is described below:

Cathode: $O_2 + 2H_2O + 4e^- \rightleftharpoons 4OH^-$ $E^e = +0.40$ V

Anode: $CO(NH_2)_2 + 6OH^- \rightleftharpoons N_2 + CO_2 + 5H_2O + 6e^-$ $E^e = -0.75$ V

Overall: $2CO(NH_2)_2 + 3O_2 \rightleftharpoons 2N_2 + 2CO_2 + 4H_2O$ $E^e_{cell} = +1.15$ V

The theoretical open circuit voltage (V_{OC}) of a DUFC is 1.15 V at room temperature, slightly lower than the 1.23 V for a H_2-O_2 fuel cell. Both cathodic reaction and anodic reaction are catalyzed by suitable catalyst, such as Pt, MnO_2, Ni or NiO for reduction of O_2 gas at cathode and Co, Ni, Cu for oxidation of urea at anode[10, 11, 12]. In this section, the Ni-doped CuZn alloy-based array electrode was designed and prepared for the anodic reaction – oxidation of urea in the neutral condition.

2.2 Materials and Experimental Conditions

2.2.1 Preparation of Cu-Zn Nanostructured Array Electrode

Chemical reagents including copper foam, zine powder and potassium peroxydisulphate ($K_2S_2O_8$ Acros) and urea were used as received without further purification. The copper hydroxide nanostructures were prepared by immersion method. A solution with $(NH_4)_2S_2O_8$ and NaOH (in mole ratio of 1 : 24) was prepared by dissolving all chemical at 4 ºC. A copper foam strip (2 cm × 4 cm) was immersed in the solution, without stirring, for 2 hrs. After the immersion, the foam was then rinsed with deionized water to remove excess NaOH or $(NH_4)_2S_2O_8$, and dried at 50 ºC[13]. The copper hydroxide nanostructures were then reduced chemically by the town gas under heating, until the copper foam strips change back to reddish brown color (Figures 2.1 (a) to (c)). The structure and morphology of nanostructured on the reduced copper foam strips were examined and studied by SEM analysis.

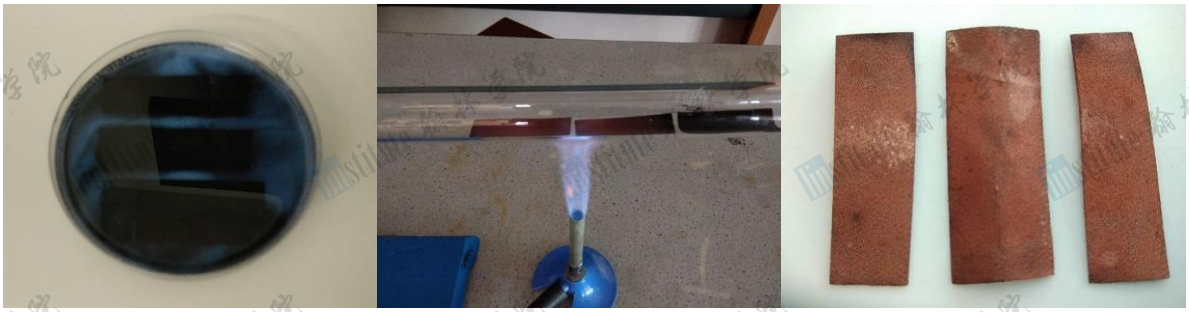

Figure 2.1 (a) Left: 3 copper foam strips immerse in the alkaline $K_2S_2O_8$ solution.

(b) Middle: oxidized copper foam strips under chemical reduction by flowing hot town gas.

(c) Right: reduced copper foam strips with nanostructure.

Converting Cu-based nanostructure to Cu-Zn alloy-based nanostructured electrode was done by the reduction of $Zn(OH)_4^{2-}$ to Zn on the surface of Cu nanostructured foam. As prepared Cu nanostructure electrodes were heated with alkaline $Zn(OH)_4^{2-}$ solution with some undissolved Zn powder, at 80 °C for 30 minutes. The mixture (Cu nanostructured foam and solution) was cooled to room temperature naturally. The sample was then heated inside the furnace at 250 °C to give Cu-Zn alloy. The final electrode was rinsed extensively with deionized water to remove any adsorbed $Zn(OH)_4^{2-}$ and NaOH(aq) on its surface. The structure and morphology of nanostructure were re-checked to ensure no structural deformation [Figures 2.2 (a) to (c)].

Figure 2.2 (a) Left: Cu foam heated with the solution of $Zn(OH)_4^{2-}$ with Zn suspension

(b) Middle: Cu-Zn foam strips after chemical treatment

(c) Right: student performing SEM analysis

Cu-Zn electrodes with different percentage of Ni-doped were synthesized by typical method mentioned below. Solutions with various Ni^{2+} concentration (0 – 20%, by mass of Cu-Zn electrode) were prepared by dissolving various amount of Ni^{2+} salt in deionized water. The Cu-Zn alloy electrode was soaked in the solution and then heated hydrothermally at 150 ºC for 6 hours. The Cu-Zn-Ni electrode was rinsed with deionized water and then dried in 45 ºC overnight.

2.2.2 Material Characterizations

Powder X-ray diffraction data were recorded by using a Rigaku SmartLab X-ray diffractometer with Cu $K\alpha_1$ irradiation (λ=1.5406 Å) at a scanning rate of 0.01º per second. The crystal size was estimated by applying the Schrerrer equation ($\Phi = K\lambda/\beta\cos\theta$), where Φ is the crystal size, λ is the wavelength of the X-ray irradiation (0.154 nm), K is usually taken as 0.89, β is the peak width at half-maximum height after subtraction of the instrumental line broadening using silicon as a standard, and θ is the diffraction angle of the (111) peak of the cubic phase. Scanning electron microscopy (SEM) measurements were carried out by using a Hitachi TM4000 plus to investigate the morphology and surface roughness of samples.

2.3 Results and Discussion

2.3.1 XRD Analysis

Phases and purities of the as-prepared samples were investigated by the XRD Analysis. Figures 2.3 show the XRD patterns of the sample at different stages. The structure of Cu-Zn alloy is characterized by the presence of peak (111) at $2\theta = 42^{o}$, characteristic of the α phase of the polycrystalline Cu-Zn alloy with a preferential orientation along the (111) plane.

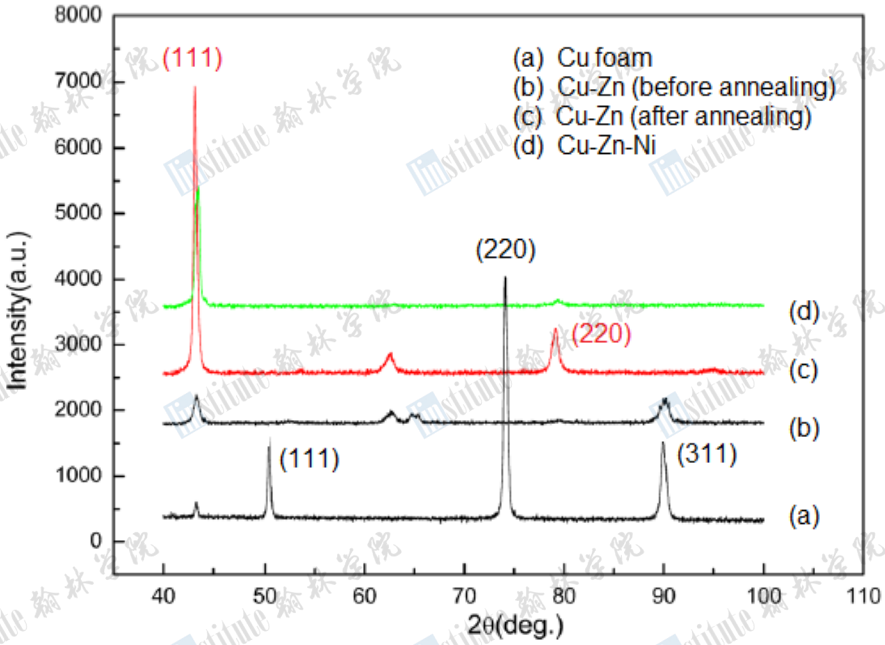

Figure 2.3 (a) to (d) XRD spectrums of sample at different stages

Figures 2.3 (a) and (b) shows the change of the structure of copper foam to Cu@Cu-Zn (before annealing) with nanostructure before annealing. Obviously, the absence of the peaks (111) and (220) at $2\theta = 51^{o}$ and 74^{o} respectively for Cu foam [Figure 2.3 (a)] and presence of peak (111) at $2\theta = 42^{o}$ for Cu@Cu-Zn [Figure 2.3 (b)] demonstrates the structural transformation from Cu to Cu-Zn alloy. Such transformation is not completed before annealing, which is confirmed by the presence of peak (311) at $2\theta = 90^{o}$ in Figure 2.3 (b) with weaker signal than the one in Figure 2.3 (a). Hence, mixing of two distinguished peaks in Figure 2.3 (b) (peak (311) for Cu and peak (111) for Cu-Zn) exhibit the metastable status of Cu-Zn alloy at this stage.

After annealing at 250 ^{o}C for 3 hours, the significant increase in signal for peaks (111) and (220) at $2\theta = 42^{o}$ and 78^{o} and absence of peak at $2\theta = 90^{o}$ represent the complete crystal structure transformation from Cu to Cu-Zn [Figures 2.3 (b) and (c)]. Furthermore, sharp and strong signal for peak (111) truly demonstrates the good crystallization of α-Cu-Zn particle on the sample. The X-ray patterns in Figures (b), (c) and (d) are characteristic of the face-centered cubic crystal structure of α-Cu-Zn (JCPDS 50-1333).

Figure 2.3 (d) shows the XRD pattern of our final sample Cu-Zn with Ni doping, which is similar as Cu-Zn. However, the signal for peaks (111) and (220) are relatively weaker and it implies that the crystallinity of Cu-Zn alloy is affected by Ni^{2+} ion embedment in the lattice during hydrothermal treatment.

2.3.2 SEM Analysis

The morphology of nanostructures at different stages (before and after chemical reduction, after Cu/Zn alloying and Ni-loading) were examined and confirmed by scanning electron microscope (SEM) analysis. Representative SEM micrographs are shown in Figures 2.4. From SEM images $Cu(OH)_2$ nanostructures were extensively grown on the copper foam on a large scale. Figures 2.4 (a) reveals uniform rod-shaped $Cu(OH)_2$ grown on the copper foam with relatively uniform width of 100 nm and lengths ranging from 5 to 7 μm (based on SEM image estimations), in bottom-to-top directions from its surface. A large aspect ratio is thus achieved in the range of 50 to 70. The $Cu@Cu(OH)_2$ nanorods were chemically-reduced by flowing hot town gas [Figure 2.1 (b)]. The morphology and shape of those nanorod are well preserved after chemical reduction, without serious structural deformation or aggregation [Figure 2.4 (b)].

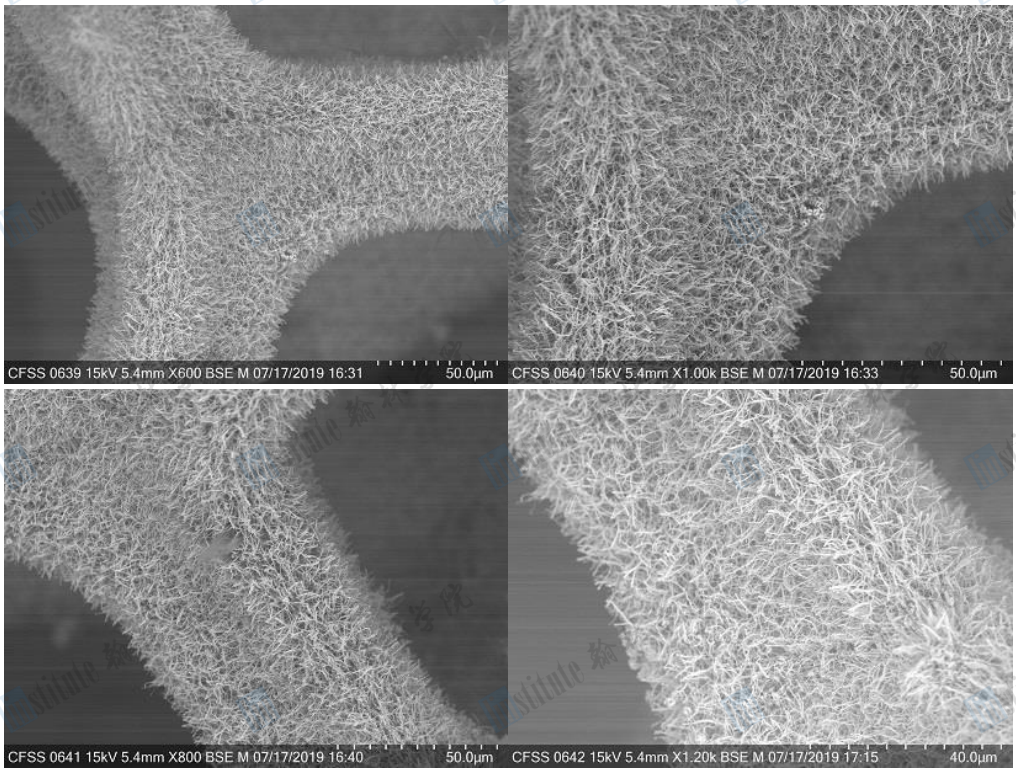

Figure 2.4 (a) Top: SEM images of $Cu@Cu(OH)_2$ nanorod array electrode, before chemical reduction

(b) Bottom: SEM images of Cu@Cu nanorod array electrode, after chemical reduction

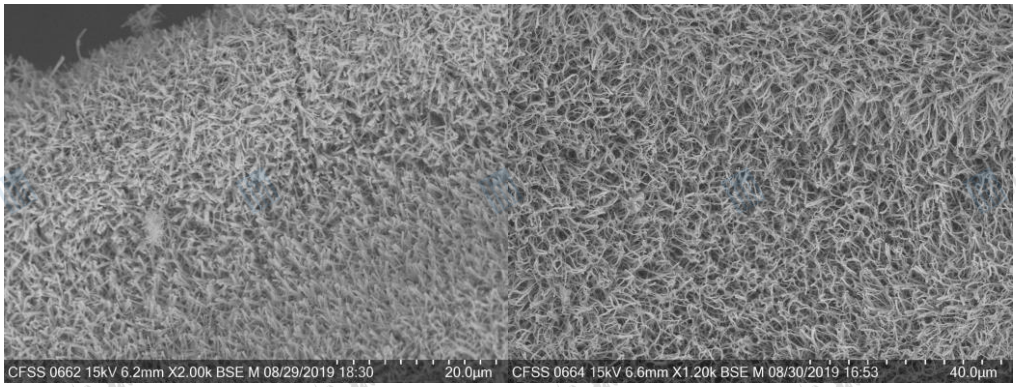

Figure 2.4 (c) Left: SEM images of Cu@Cu-Zn nanorod array electrode, after alloying

(d) Right: SEM images of Cu@Cu-Zn-Ni nanorod array electrode, after Ni doping

The morphology of those nanorods are even preserved without deformation after treating with hot alkaline $Zn(OH)_4^{2-}$ solution for 30 min, followed by annealing up to 250 °C for 2 hours [Figure 2.4 (c)]. From those SEM images, no Zn nanoparticles trapped in the space between nanostructures, and conclude that Zn coating is relatively uniform and homogenous. Finally, samples were then treated with Ni^{2+} solution hydrothermally for doping. Figure 2.4 (d) clearly exhibits a clear and clean nanorod structure on the copper foam.

The orderly alignment of nanorods on the copper foam provides hierarchical structure with both macropores and mesopores, with extensive resistance-free pathway, which facilitate the diffusion of ions or molecules between electrode and diffusion layer of solution film, and large surface area-to-volume ratio for redox reactions. In conclude, Cu-Zn-Ni nanorods can be fabricated by chemical oxidation of Cu by alkaline $(NH_4)_2S_2O_8$, followed by CH_4/H_2 gas reduction, Zn alloying in alkaline condition and Ni doping [Figure 2.4 (e)].

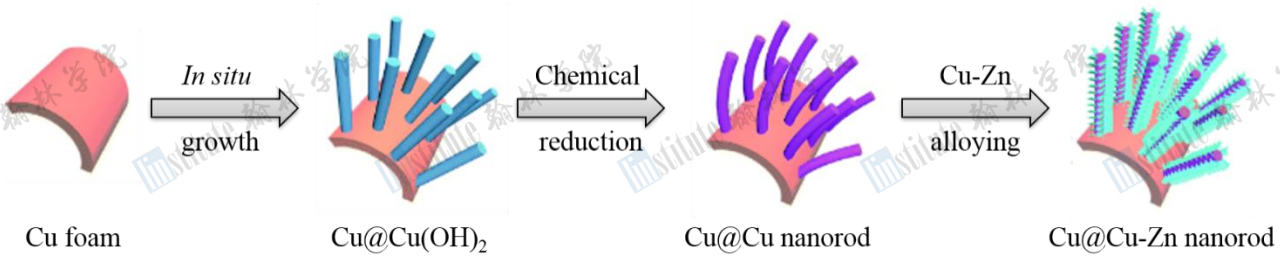

Figure 2.4 (e) Schematic diagram of synthesis of Cu-Zn nanorod on copper foam

2.3.3 EDX and Elemental Mapping Analysis

The composition and elemental distributions of Cu@Cu, Cu@Cu-Zn and Cu@Cu-Zn-Ni were examined by SEM/EDX mapping. Figures 2.5a are the image of elemental mapping of Cu@Cu. The atomic ratio of Cu to O is 97 : 3 which indicates that the reduction of $Cu@Cu(OH)_2$ is almost completed. Figures 2.5b display the distribution of O, Cu and Zn elements in Cu@Cu-Zn, both Cu and Zn are homogeneously distributed over the electrode with Cu : Zn : O atomic ratio of 55.3 : 34.7 : 10.0 determined by EDX. The formula of the sample can be denoted as $Cu_{0.55}Zn_{0.35}O_{0.1}$. As the copper foam is used as the substrate and the signal for Cu should be dominant. Compared to the composition of Cu@Cu, sample before Zn alloying, the percentage of O increases from 3% to 10% after alloying [Figure 2.5 (b)] which may be caused by the partial oxidation of Cu-Zn alloy during annealing. Figures 2.5 (c) give an elemental mapping image of Cu@Cu-Zn-Ni after the Ni-doping. Obviously, the signal for Ni is much weaker than that of Zn and Cu, and Ni is evenly distributed over the surface of electrode. The formula of the sample is $Cu_{0.57}Zn_{0.35}Ni_{0.08}$.

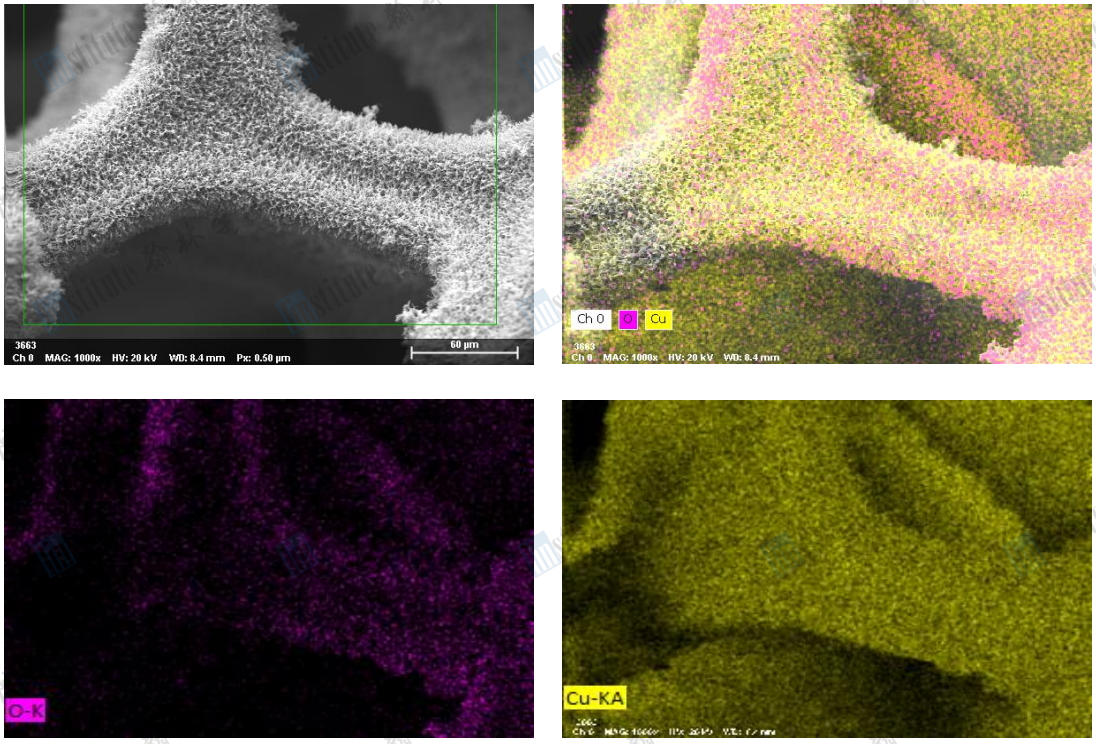

Figure 2.5 (a) SEM/EDX elemental mapping analysis of Cu@Cu, after chemical reduction

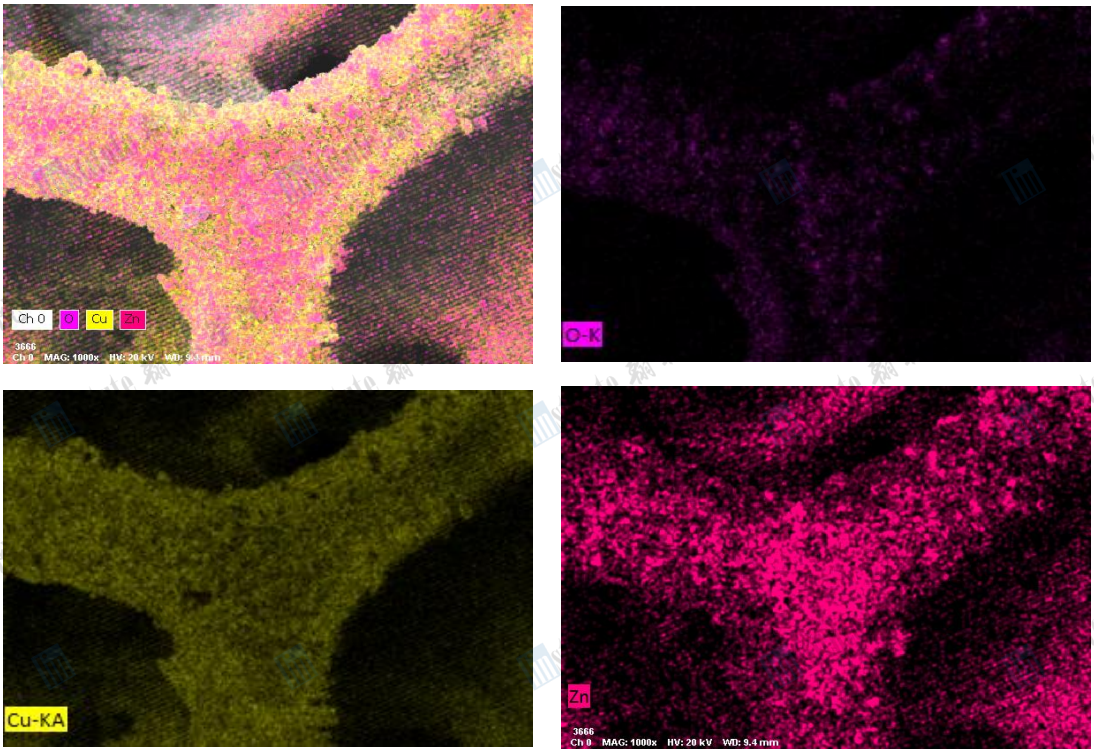

Figure 2.5 (b) SEM/EDX elemental mapping analysis of Cu@Cu-Zn, after Zn alloying

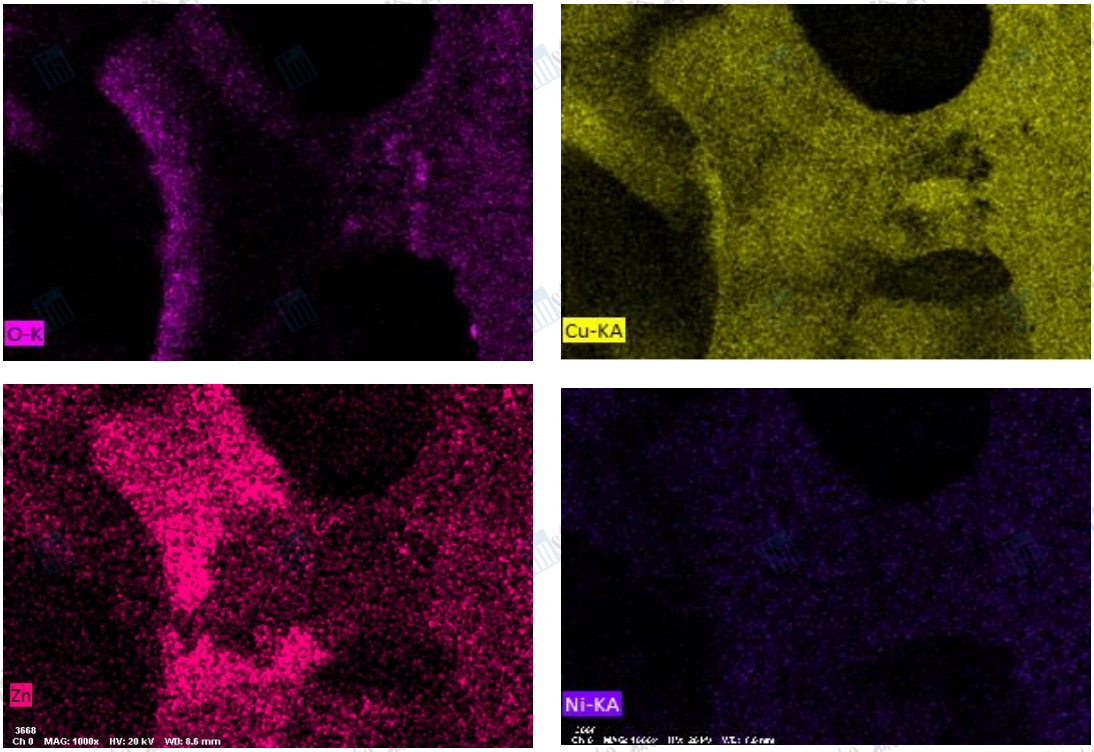

Figure 2.5 (c) SEM/EDX elemental mapping analysis of Cu@Cu-Zn-Ni

Section III Preparation of Carbon-Quantum Dot, CQD-load Air Cathode

3.1 Introduction

A simple and high efficiency carbon-based catalyst can be prepared from derivation of various biomass such as carbonization of eggplant, coconut shell, cellulose, or hydrothermal treatment of carbohydrates like glucose, sucrose or gelatin. In this project, carbon quantum dot (CQD) was prepared from gelatin by carbonizing at relatively low temperature with the help of hydrothermal treatment. The as-prepared CQD are generally small carbon nanoparticle with the size less than 10 nm. The carbon particles act as the bifunctional catalysts for the oxygen reduction and the oxygen evolution reaction occurred in the air electrode.

CQD-loaded air cathode can be easily constructed by a simple one-step, phase inversion process, using a poly(vinylidene fluoride), PVDF binder and CQD-loaded carbon black as catalyst. The phase inversion process enabled air cathode preparation at room temperatures, without the need for additional heat treatment.

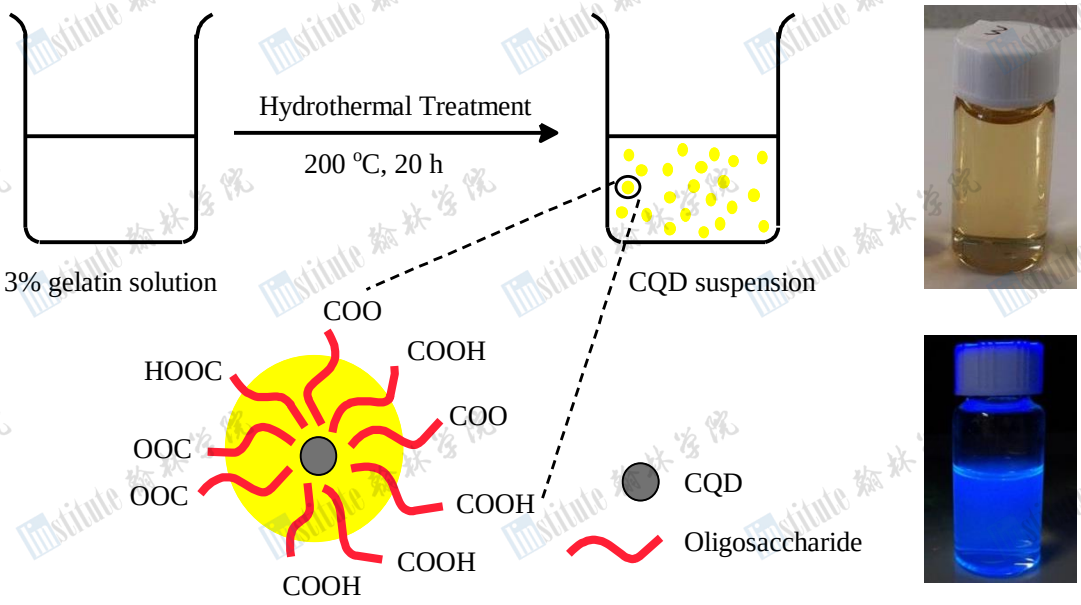

Figure 3.1 Synthesis of carbon quantum dot from gelatin

3.2 Materials and Experimental Conditions

3.2.1 Preparation of carbon quantum dot by carbonization of gelatin

Typically, 1.0 g gelation powder was dissolved in 30 cm^3 DI water with gentle heating and vigorous stirring to give 3% wt gelatin solution, followed by hydrothermal treatment in a Teflon-lined stainless-steel

autoclave at 200 °C for 20 h. After being naturally cooled, the brownish dispersion was centrifuged at 3000 rpm for 15 min to remove the sediment. The clear pale yellow supernatant was dialyzed using a dialysis tube (molecular weight cutoff: 10,000 Da) in deionized water overnight. Finally, the purified CD solution was filtered using a 0.22 μm membrane filter and freeze-dried for characterizations. The obtained brown product was dispersed in DI water to form a clear suspension with a concentration of 5 mg cm^{-3} for the subsequent fluorescent sensing measurements (Figures 3.2). Fluorescence properties of CQDs were conducted by ultra-violet spectrophotometry.

Figure 3.2 (a) Left: Appearance of CQDs solutions obtained after hydrothermal synthesis

(b) Right: Appearance of CQDs solution under the white light and UV light (365 nm) illumination

3.2.2 Preparation of CQD-load Air Cathode

Typically, 10% CQD-load carbon black, C/CQD, as the cathodic material was prepared by mixing 4 mg CQD powder and 36 mg carbon black in 20 cm^3 of absolute ethanol under 15 min sonication. After sonication, black solution was completely dried at 100 ºC. 40 mg of C/CQD powder was then mixed with 1 cm^3 10% PVDF solution (in DMF) and stirred mechanically until a homogenous black paste was given. Such black paste was loaded on the nickel foam, as the substrate, with the dimension of 2 cm × 2 cm to give an air cathode (specific areal density: 10 mg cm^{-2}). PVDF polymer film was then formed by one-step phase inversion process, immersing a whole as-prepared air cathode in deionized water for 15 min at room temperature, followed by air dry [Figures 3.3 (a) to (f)].

Figure 3.3 (a) Left: mixing CQD and carbon black to give a homogenous solid mixture

(b) Right: loading C/CQD paste on the nickel foam as the current collector

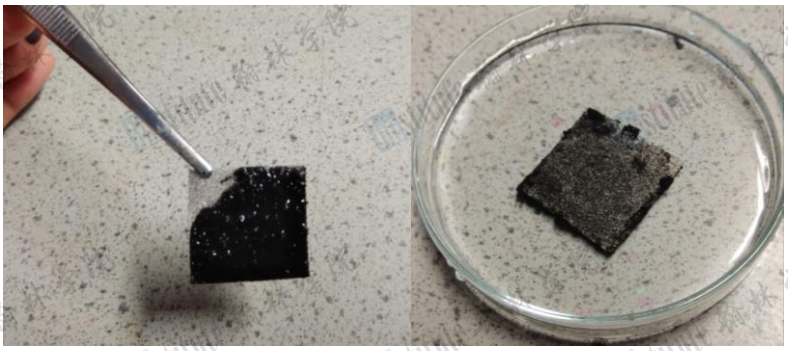

Figure 3.3 (c) Left: 2 cm × 2 cm C/CQD air cathode with areal density of 10 mg cm^{-2}

(d) Right: immersing C/CQD air cathode in DI water for phase inversion

Figure 3.3 (e) Left: drying C/CQD air cathode in the air

(f) Right: C/CQD discs with 6 mm diameter were fixed in DUFC

3.3 Results and Discussion

3.3.1 Photoluminescence of Sample

Figures 3.2 shows optical image of CQDs illuminated under white (left: daylight lamp) and UV light (right: 365 nm). The bright blue photoluminescence of CQD is strong enough to be easily seen with the naked eyes. To further confirm the formation of CQDs and the optical properties of as-synthesized CQDs, a detailed photoluminescence, PL, study was carried out by using different excitation wavelengths. Figure 3.4 shows the PL spectra of the as-synthesized CQDs with excitation at 405 and 500 nm respectively. The CQDs generated peak photoluminescence over an excitation waveband of 405 nm to 500 nm, with the peak maximum at 500 nm. All samples show the distinguished emission peak from 450 nm to 600 nm, with the peak maximum at 500 nm.

It is found that the blue photoluminescence of CQD loss if the temperature or duration of hydrothermal treatment increases. This dramatic change can be rationalized from the increasing size of CQD under the prolonged hydrothermal treatment at higher temperature. This explanation can be further supported from the formation of black carbon particle. Formation of carbon particles serves as the evidence of aggregation of millions carbon nanoparticle. Decrease in the homogeneity of solution may be another reason for the loss of the optical properties of CQD solution.

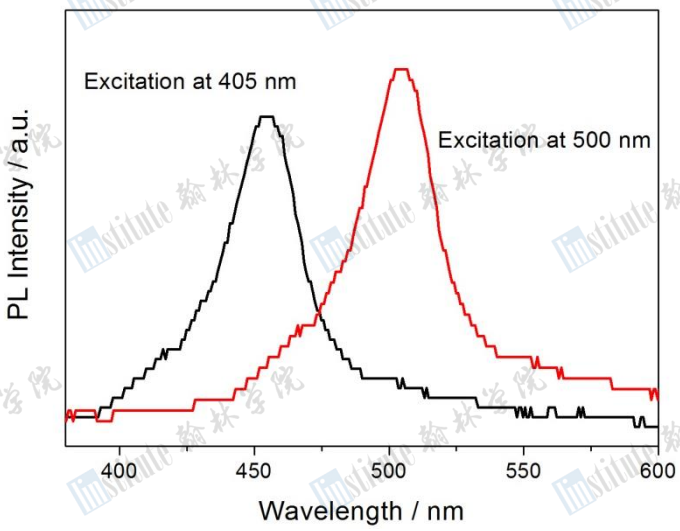

Figure 3.4 PL spectra of CQDs with excitation at 405 nm and 500 nm respectively.

Section IV Assembly of Wearable Direct Urea Fuel Cell

4.1 Assembly Procedures of Wearable Direct Urea Fuel Cell

Two type of thin, flexible and bendable energy harvesting protype models were prepared in this project: polyester-based and hydrogel-based direct urea fuel cell, DUFC (Figures 4.1). Owing to the consideration of flexibility, permeability to fuel and air and ability of water-retention, a commercially available polyester fibric or hydrogel film was chosen as substrate to provide a platform for fixing the circuit with electrodes and preserving fuel (Figures 4.1).

Figure 4.1 (a) Left: polyester fabric-based DUFC

(b) Right: hydrogel-based DUFC

Typically, polyester fabric or hydrogel with the dimension of (4 cm × 7 cm) was prepared. Copper strips were fixed on the fabric to give a circuit with the particular patterns. The discs with the diameter of 6 mm of electrodes (Cu@Cu-Zn-Ni anode and air cathode, C/Pt) were punched and fixed on the copper strips using double-sides conductive adhesive tape. The electrical conductivity of the circuit was regularly checked to ensure that the resistance of both electrode paths was less than 20 Ω [Figures 4.2 (a) to (h)]. The performances of flexible DUFC were tested under different situations such as change in pH, concentration of urea, bending angles, using artificial sweat and true sweat etc [Figures 4.2 (i) and (j)].

Figure 4.2 (a) Left: electrode discs with 6 mm diameter were punched

(b) Right: fixing the metal strip (copper or nickel) to give a circuit

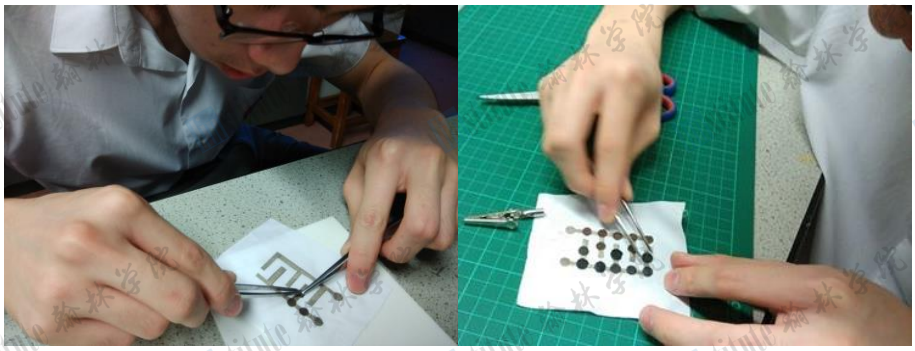

Figure 4.2 (c) Left: electrode discs were fixed on the copper strips

(d) Right: Cu@Cu-Zn as the anode and C/Pt as the air cathode

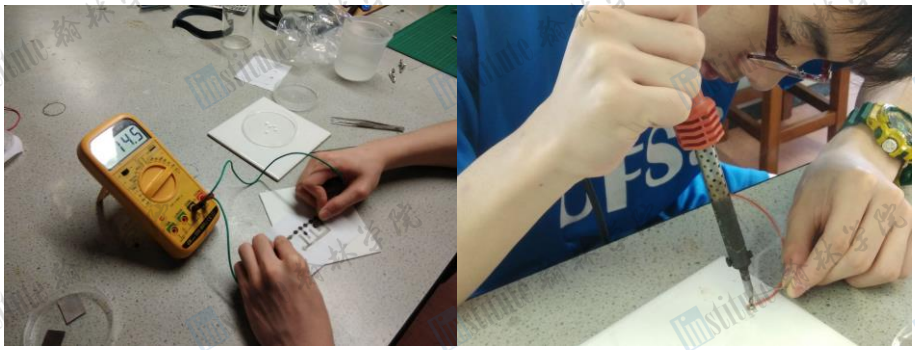

Figure 4.2 (e) Left: checking the electrical resistance of the circuit

(f) Right: soldering copper wire to the adhesive disc

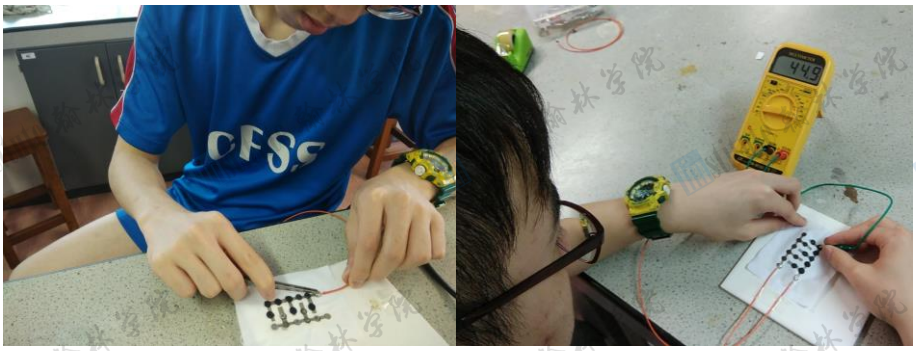

Figure 4.2 (g) Left: fixing the copper disc to the circuit with electrode discs

(h) Right: checking the electrical resistance of the circuit

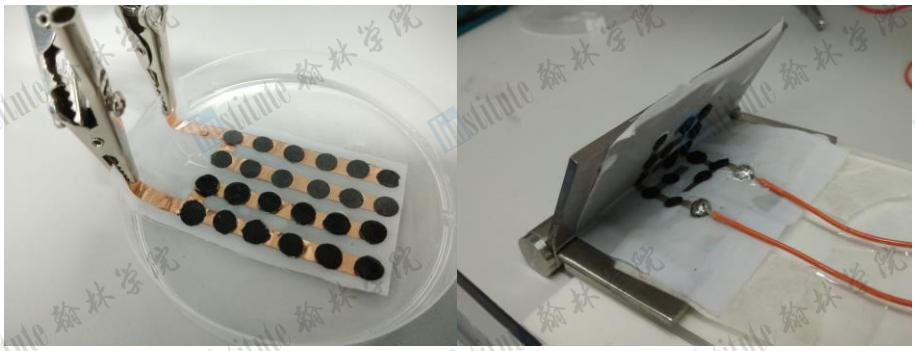

Figure 4.2 (i) Left: polyester-textile based DUFC was under testing

(j) Right: flexible DUFC was bended at different angle.

Section V Electrochemical Performance of Wearable Direct Urea Fuel Cell

5.1 Introduction

In this section, a series of DUFC were prepared to investigate the effects of temperature, pH environment, concentration of electrolyte, type of cathode, anode on the electrochemical performance. The operating mechanism of a DUFC using an alkaline membrane electrolyte is describe below:

Cathode: $O_2 + 2H_2O + 4e^- \rightleftharpoons 4OH^-$ $E^e = +0.40$ V

Anode: $CO(NH_2)_2 + 6OH^- \rightleftharpoons N_2 + CO_2 + 5H_2O + 6e^-$ $E^e = -0.75$ V

Overall: $2CO(NH_2)_2 + 3O_2 \rightleftharpoons 2N_2 + 2CO_2 + 4H_2O$ $E^e_{cell} = +1.15$ V

The reduction of oxygen in air is catalyzed by expensive metal such as Pt or other transition metal oxide, MnO_2 or NiO etc. at cathode in the alkaline condition, while urea in urine or sweat acts as fuel and is oxidized to N_2 and CO_2. The theoretical open circuit voltage (V_{OC}) and the efficiency of hydrogen and urea fuel cells at 298 K are +1.15V at room temperature, slightly lower than the +1.23 V for a H_2/O_2 fuel cell, while the theoretical efficiency of a urea fuel cell is almost 100% at 298 K which is about 20% higher than that of H_2/O_2 fuel cell (83%). The high theoretical efficiency of a urea fuel cell is due to the positive entropy change of the overall reaction.

5.2 Electrochemical Performance of Wearable Direct Urea Fuel Cell

The electrochemical performances of as-prepared DUFC were investigated by ZKE EBC-A10H battery capacity tester to determine the power capacity and energy capacity of a unit cell under different conditions. Artificial sweat buffered at pH 7.2 was used as the matrix and prepared by dissolving various type of salts (NaCl, $MgSO_4$, K_2CO_3 and $CaCl_2$) according to the Figure 5.1.

Type of cation	Mg^{2+}	Ca^{2+}	K^+	Na^+
concentration	1 mM	1 mM	8 mM	50 mM

Figure 5.1 Composition of artificial sweat

5.3 Results and Discussion

5.3.1 Effect of Anode and its Optimum Working pH Environment

The focus of this part is to study the effect of working pH environment towards the overall performance of DUFC using Cu@Cu-Zn and C/Pt as anode and cathode respectively. pH of the artificial sweat with 0.33 M urea was adjusted from 1 to 13. The open circuit and specific power density were followed during the course of the experiment.

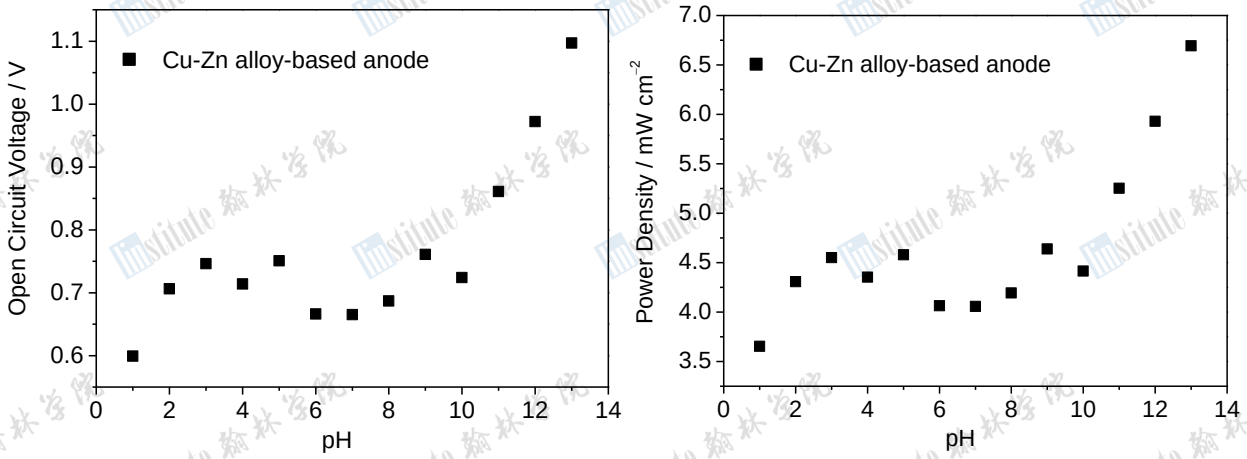

Figure 5.1 (a) Left: Open circuit voltage of DUFC (anode: Cu@Cu-Zn, cathode: C/Pt)

(b) Right: Specific power density of DUFC

Figures 5.1 (a) to (c) show the distribution of open circuit voltage (V_{OC} in V) and specific power density in mW cm^{-2} obtained in various pH environment. In general, the performances of DUFC of various samples are pH-dependent and the output power density always increases with increasing pH. The output specific power density of DUFC increases from 3.65 mW cm^{-2} (in pH 1.0) to 6.69 mW cm^{-2} (in pH 13.0), showing 83% increment.

pH	V_{OC} / V	Power density / mW cm^{-2}	pH	V_{OC} / V	Power density / mW cm^{-2}
1	0.599	3.65	8	0.687	4.19
2	0.706	4.31	9	0.761	4.64
3	0.746	4.55	10	0.724	4.42
4	0.714	4.35	11	0.861	5.25
5	0.751	4.58	12	0.972	5.93
6	0.666	4.06	13	1.097	6.69
7	0.665	4.06			

Figure 5.1 (c) Performance of DUFC (anode: Cu@Cu-Zn, cathode: C/Pt) at different pH environment

The improved performance in DUFC can be rationalized from shifting of the equilibrium state of the corresponding redox reaction. Referring to the anodic reaction – oxidation of urea, increasing the concentration of OH^- in higher pH environment definitely can shift the equilibrium position to the right (product side) to further increase is reduction potential.

Anode: $CO(NH_2)_2 + 6OH^- \rightleftharpoons N_2 + CO_2 + 5H_2O + 6e^-$ $E^\ominus = -0.75$ V

Moreover, high pH environment favors the dissolution of carbon dioxide gas that further prevent the polarization of electrode, leading the decline of output potential. Although better performance of DUFC can be achieved, owing to the pH of sweat always lies from 6.5 to 7.5, neutral working pH environment was chosen as the final choice.

5.3.2 Effect of Temperature of the Anodic Electrolyte

An ideal DUFC could be able to maintain its excellent performance through a wide range of environmental temperature. In order to achieve this, discharging analysis for DUFC was further conducted at a temperature from 5 °C to 95 °C. Anodic electrolyte (0.33 M urea) in the reservoir was hold with constant heating and stirring. The output voltage and power were measured at the constant temperature interval.

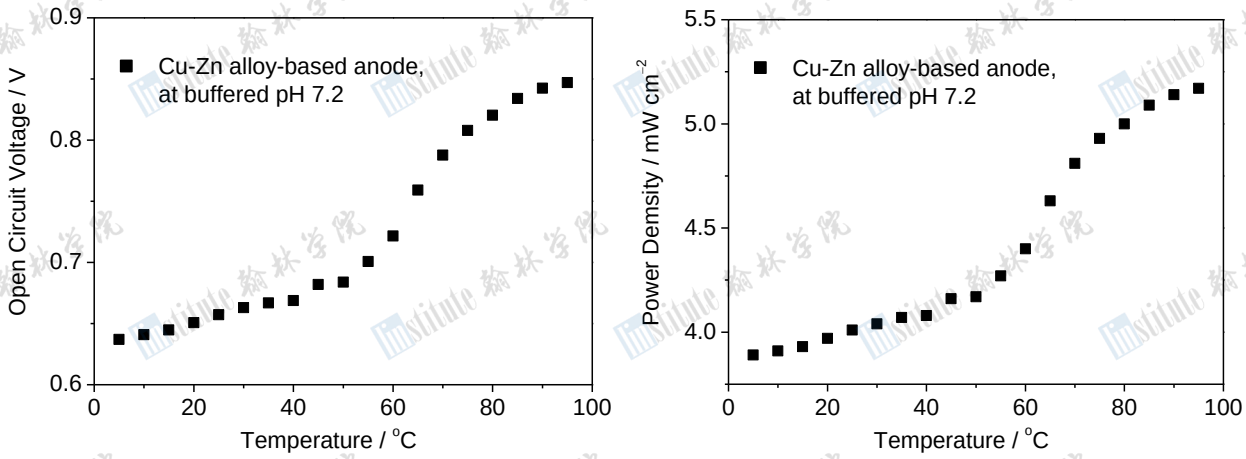

Figure 5.2 (a) Left: Open circuit voltage of DUFC (anode: Cu@Cu-Zn, cathode: C/Pt)

(b) Right: Specific power density of DUFC

pH	V_{OC} / V	Power density / mW cm^{-2}	pH	V_{OC} / V	Power density / mW cm^{-2}
5	0.637	3.89	55	0.701	4.27
10	0.641	3.91	60	0.722	4.40
15	0.645	3.93	65	0.759	4.63
20	0.651	3.97	70	0.788	4.81
25	0.657	4.01	75	0.808	4.93
30	0.663	4.04	80	0.820	5.00
35	0.667	4.07	85	0.834	5.09
40	0.669	4.08	90	0.842	5.14
45	0.682	4.16	95	0.847	5.17
50	0.684	4.17			

Figure 5.2 (c) Performance of DUFC (anode: Cu@Cu-Zn, cathode: C/Pt) at different temperature

From the results [Figures 5.2 (a) to (c)], they showed that DUFC exhibits a fairly constant output power and retains in the range of 3.8 – 4.3 mW cm^{-2} till the temperature reaches 60 °C. Beyond 60 °C, output power density climbs to 5.2 W dm^{-3} at 95 °C, showing 278% increment. It is no doubt that the DUFC exhibits and demonstrates a stable performance over a wide range of temperature from room temperature up to 60 °C. Although higher temperature shows properties that are more outstanding in power density, temperature of sweat should be same as room temperature at thermal equilibrium, hence, 25 °C was selected as experimental parameter for following test.

5.3.3 Effect of Concentration of Urea

The concentration of urea in the industrial sewage or urine from human or animal usually are in the range of 2wt% to 6 wt%, which is equivalent to 0.33 M to 1 M. The ideal DUFC should able to perform normally and be sensitive in the low concentration of urea in sweat. Hence, the urea-containing sewage or excretion from animal and human can be a source of fuel for generating electricity by DUFC. The focus on this part is to investigate the sensitivity of DUFC towards range the concentration of urea in artificial sweat. A series of standard urea solution were prepared, with the concentration of urea from 0.02 M to 0.9 M. All of them are buffered at pH 7.2 for comparison. Figures 5.3 show the percentage change of open circuit voltage and specific power density with the concentration of urea. Our DUFC model displays the significant change in voltage and power density when the concentration of urea up to 0.08 M, and the percentage change becomes steady at

+300% when the artificial sweat contains 0.9 wt% (0.15 M) of urea. Hence, our DUFC is practical and able to perform functionally in the real situation with low urea concentration.

[Urea] / M	V_{OC} / V	Power density / mW cm^{-2}	% change
0.00	0.128	0.78	0
0.02	0.256	1.56	+100
0.04	0.361	2.20	+182
0.08	0.437	2.66	+241
0.15	0.538	3.28	+320
0.30	0.646	3.93	+405
0.45	0.653	3.98	+410
0.60	0.664	4.04	+419
0.75	0.673	4.10	+426
0.90	0.668	4.07	+422

Figures 5.3 (a) Performance of DUFC with the function of concentration of urea

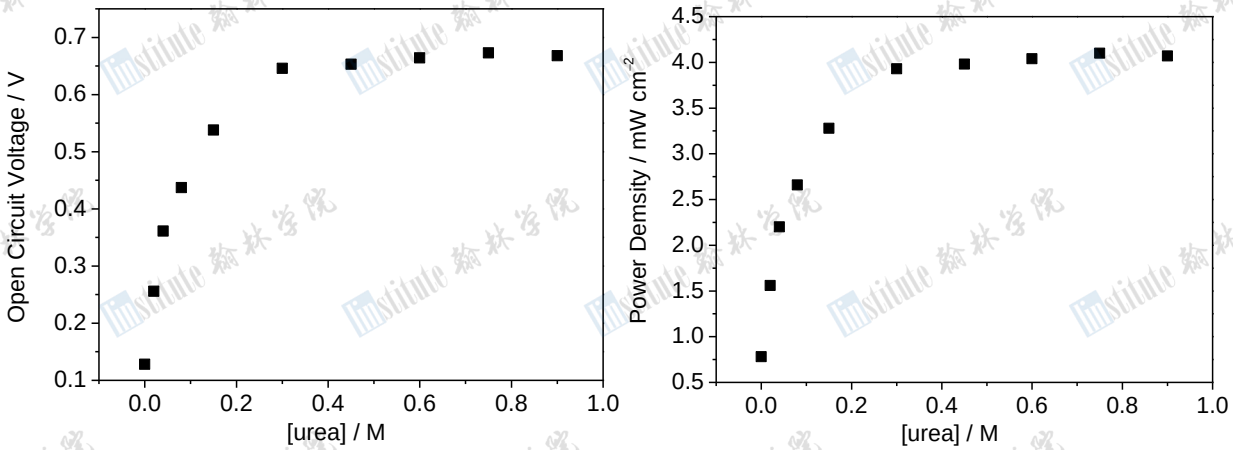

Figure 5.3 (b) Left: Open circuit voltage of DUFC (anode: Cu@Cu-Zn, cathode: C/Pt)

(c) Right: Specific power density of DUFC

5.3.4 Effect of Nanostructure of Cu@Cu-Zn Anode

The effect of nanostructure of Cu@Cu-Zn anode was extensively investigated. Two sets of comparison were made: (1) bare copper foam, Cu@Cu and copper foam with copper nanostructure, nanostructured Cu@Cu; and (2) copper foam with Zn alloying, Cu@Cu-Zn, and nanostructured Cu@Cu-Zn. Figure 5.4 displays the change in open circuit voltage with time. Whatever the type of materials (Cu or Cu-Zn alloy), anode with nanostructured materials shows a better performance with 41% and 16% enhancement respectively.

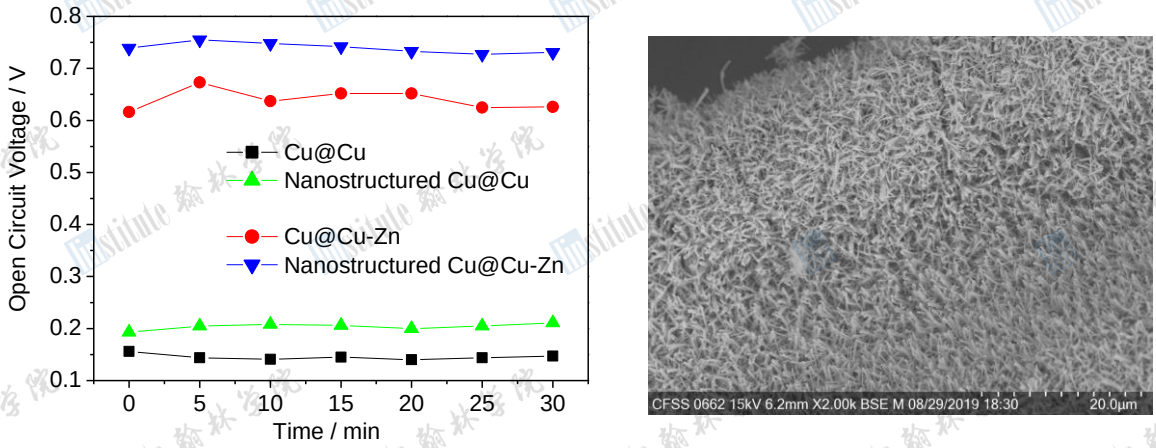

Figure 5.4 (a) Left: Change in open circuit voltage of DUFC with time

(b) Right: SEM image of nanostructured Cu@Cu-Zn anode

The extraordinary performance can be rationalized from the presence of nanostructure of either Cu or Cu-Zn and their orderly alignment of nanostructure on the copper foam providing hierarchical structure with both macropores and mesopores with extensive resistance-free pathway, which facilitate the diffusion of ions or molecules between electrode and diffusion layer of solution film, and large surface area-to-volume ratio for redox reactions over the surface of electrode.

5.3.5 Effect of Ni-doping on Cu@Cu-Zn Anode

Various amount of Ni (0% to 20%, by weight) were doped into nanostructured Cu@Cu-Zn anode by using hydrothermal treatment method, as mentioned in Section 2.2.1. Figure 5.5 (a) exhibits more superior performance in output voltage if the Cu@Cu anode was replaced by Cu@Cu-Zn, showing 262% increases, while further 18% increment was contributed by 8% Ni doping on Cu@Cu-Zn anode. Similar results were shown in Figure 5.4 (b), its performance climbs to 0.874 V (8% Ni-doping) and then level off. The optimum percentage of Ni-doping lies on the range of 6% to 10%.

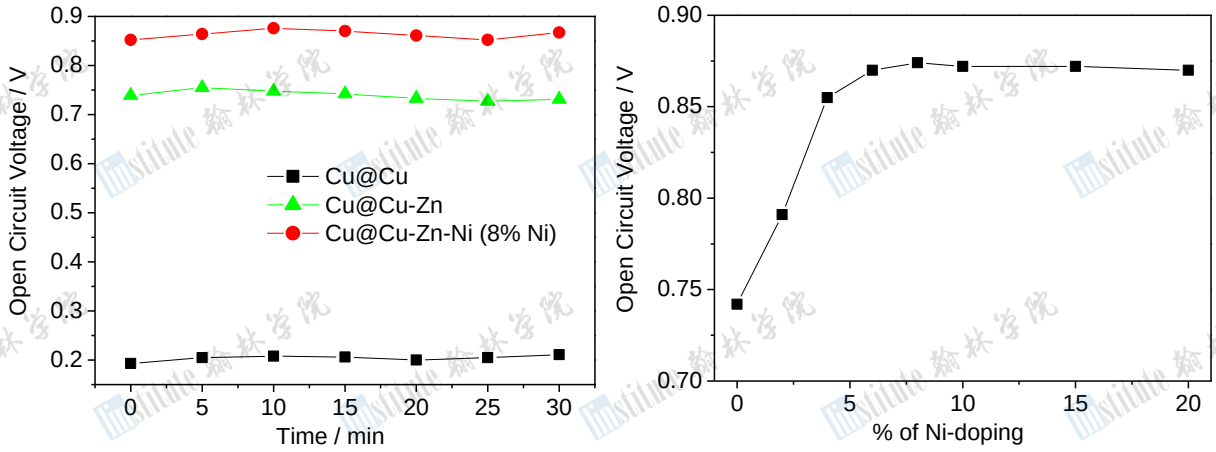

Figure 5.5 (a) Left: Change in open circuit voltage of different structure of anode with time
(b) Right: Change in open circuit voltage of DUFC with different percentage of Ni-doping on Cu@Cu-Zn anode

Figures 5.5 (c) and (d) shows the measured polarization curves of the DUFC using nanostructured Cu@Cu-Zn-Ni anode with different percentage of Ni-doping. It can be seen that the measured voltages, including the open-circuit condition, increased as the percentage of Ni-doping. All samples outperformed the 0% Ni-doping sample's onset potential, indicating higher activity because of the Ni-doping effect. The maximum cell performance was achieved for an anode with 10% Ni-doping (peak power density 15.16 mW cm^{-2} at current density of 32 mA cm^{-2}, with 275% increases). At low current densities, cell performance for 10% Ni-doping resembled that of 8% Ni-doping, with similar open-circuit voltage. However, above 15 mA cm^{-2} the cell performance for 10% surpass others as the limited amount of Ni-catalyst assessable on anode in other fuel cells. More drastic results were evident at higher current density up to 30 mA cm^{-2}. Figure 5.5 (e) shows the variation of maximum power density of the cell with wide range of percentage of Ni-doping, from 0% to 20%. The cell performance climbs drastically from 0% to 10% Ni-doping, and then levels off.

To summarize, the performance improved with increasing percentage of Ni-doping, which can be rationalized from the high disorder structure of Cu-Zn lattice that provide more catalytic site for the oxidation of urea. Compared to other samples with higher percentage of Ni-doping, 10% Ni-doping was shown to be competitive, and their lower material costs make them an efficient catalyst for our DUFC.

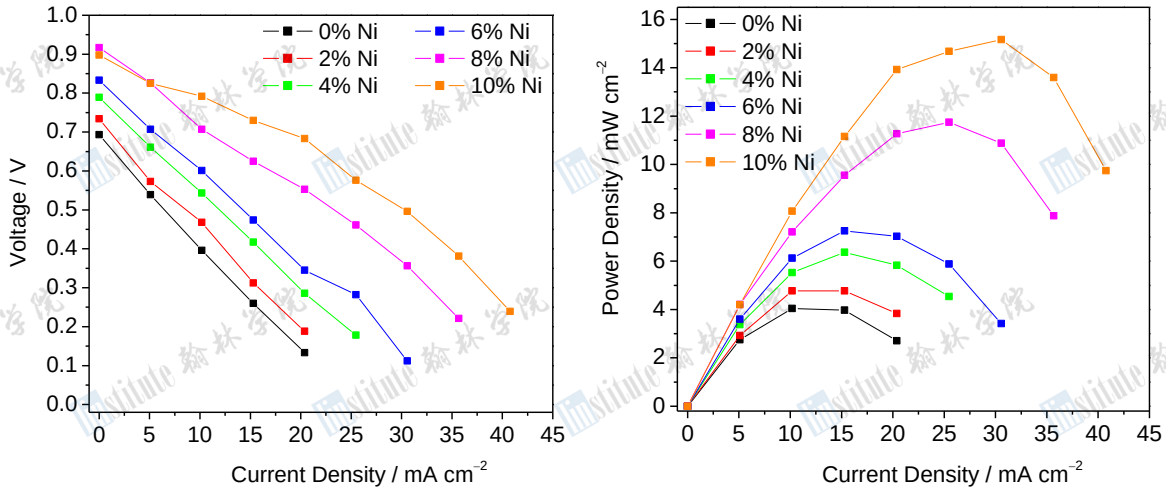

Figure 5.5 (c) Left: Polarization curve of different DUFC model, in term of cell voltage
(d) Right: Polarization curve of different DUFC model, in term of power density

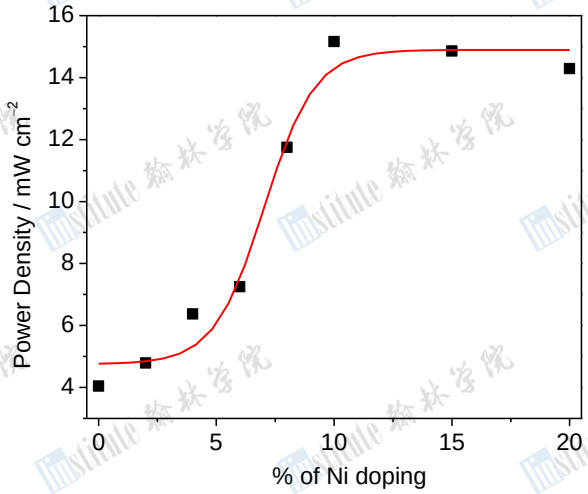

% of Ni	Power density, mW cm^{-2}
0	4.04
2	4.79
4	6.37
6	7.25
8	11.75
10	15.16
15	14.86
20	14.29

Figure 5.5 (e) Change in power density of DUFC with different percentage of Ni-doping on Cu@Cu-Zn anode

5.3.6 Alternative catalyst for air cathode

The feasibility of using urea as the energy source in DUFC and effect of anode have been demonstrated in the previous studies, using commercially available C/Pt as the reference cathode. Since precious expensive platinum catalyst is used in the cathode for facilitating oxygen reduction reaction (ORR), which is economically unsound. In view of this, the carbon-based catalyst, carbon quantum dots, CQDs, were prepared via hydrothermal treatment of gelatin, as mentioned in Section 3.2.1. For comparison, commercially available 10% C/Pt air cathode was selected as the reference. Two types of DUFC were prepared by using either 10% C/Pt or 10% C/CQD as air cathode and using 10% Ni-doped Cu@Cu-Zn as anode.

Figures 5.6 (a) and (b) shows the change in open circuit voltage with time and discharge curve under constant current of DUFCs using different air cathode. Basically, the performance of two model (C/Pt or C/CQD) are comparable. From the discharge curves in Figure 5.6 (b), both samples show about 0.1 V losses (activation losses) caused by the slowness of the reaction taking place on the surface of the electrodes. Hence, a proportion of the voltage generated is lost in driving the chemical reaction that transfers the electrons. Later on, change in output voltage steps into the ohmic losses that the voltage drop due to the resistance to the flow of electrons through the material of the electrodes. Two models demonstrate a steady ohmic losses for 0.35 V in 60 min. Finally, the sudden drop in output voltage results from the change in concentration of reactants at the surface of electrodes as the fuel (urea) is used. Performance and capacity of two models are shown in Figure 5.6 c.

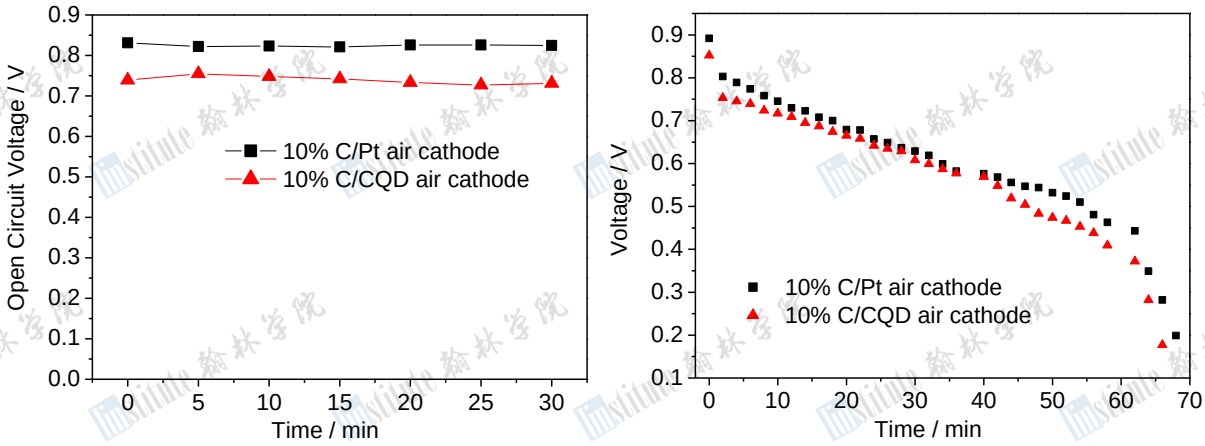

Figure 5.6 (a) Left: Change in open circuit voltage of different air cathode with time
(b) Right: Discharge curves of DUFC using C/Pt and C/CQD air cathode, under constant current, 1 mA

Anode	10% Ni-doped Cu@Cu-Zn	
Cathode	10% C/Pt	10% C/CQD
V_{OC}, V	0.892	0.852
Capacity, mAh	47	43
Energy capacity, mWh	20	17
Power density, mW cm^{-2}	15.16	14.26

Figure 5.6 (c) Performance of DUFC C/Pt and C/CQD air cathode

The effect of different type air cathode was further investigated from the polarization curves of these two DUFCs, shown in Figures 5.6 (d) and (e). Both models display the similar pattern of polarization curve whatever the type of air cathode was used. The maximum cell performance was achieved for a C/Pt air cathode and C/CQD air cathode with peak power 15.16 mW cm^{-2} and 14.26 mW cm^{-2} at current density of 32 mA cm^{-2} respectively. To summarize, from the polarization curve and discharge curve of two models, it concluded that the performance of DUFC using C/CQD air cathode is comparable to that of using C/Pt as air cathode. Hence, using carbon-based CQD as the catalyst in cathode opens up the possibility of development of green DUFC for new generation.

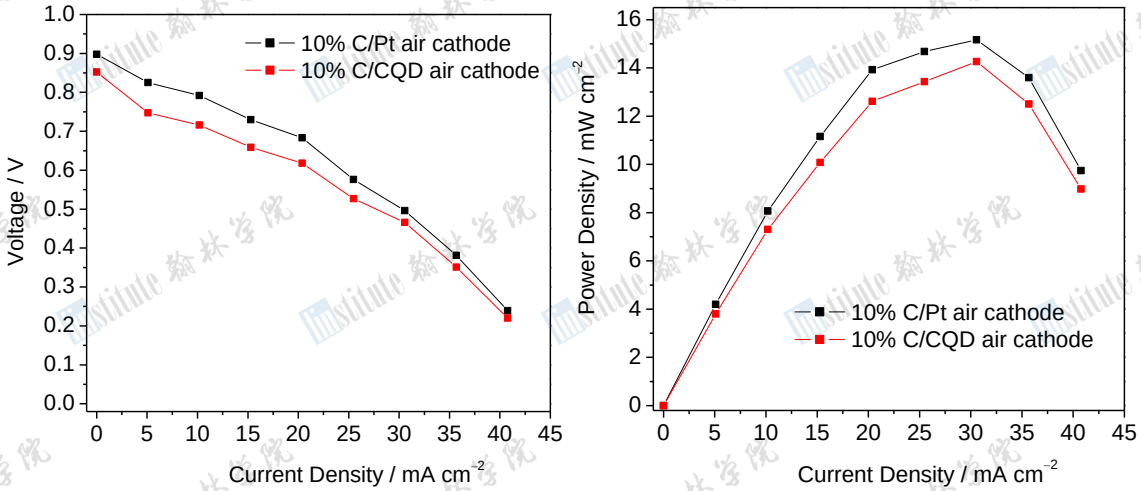

Figure 5.6 (d) Left: Polarization curve of different DUFC model, in term of cell voltage
(e) Right: Polarization curve of different DUFC model, in term of power density

Section VI Practical Trial

6.1 Introduction

Fabricating wearable, flexible DUFC using sweat as the fuel is the ultimate goal of this project. In this section, the prototype DUFC was tested under a real situation, adhering on the different parts of body (front arm, chest and shoulder blade) and using sweat as the fuel for generating electricity, At the same time, performance of DUFC will also be studied in different postures by experimenter (Figure 6.1).

Anode	10% Ni-doped Cu@Cu-Zn	
Cathode	10% C/Pt	10% C/CQD
Fuel	Sweat	
Substrate	Polyester fabric / hydrogel film	
Body part	Front arm / chest / shoulder blade	
Action	Muscle contraction / relaxation / under pressure	
Body posture	Straight / bend	

Figure 6.1 Experiment parameters of practical trial

6.2 Result and Discussion

6.2.1 Performance of DUFC at different bending angle

DUFC protype was bended at different angle, and its open circuit voltage was measured once the reading kept steady (Figure 6.2). Obviously, there is no serious deterioration or drop in the output voltage and its performance maintain fairly constant at different bending angle. This is particularly crucial as the wearable energy harvesting device should be able to function normally under different level of activity or body posture.

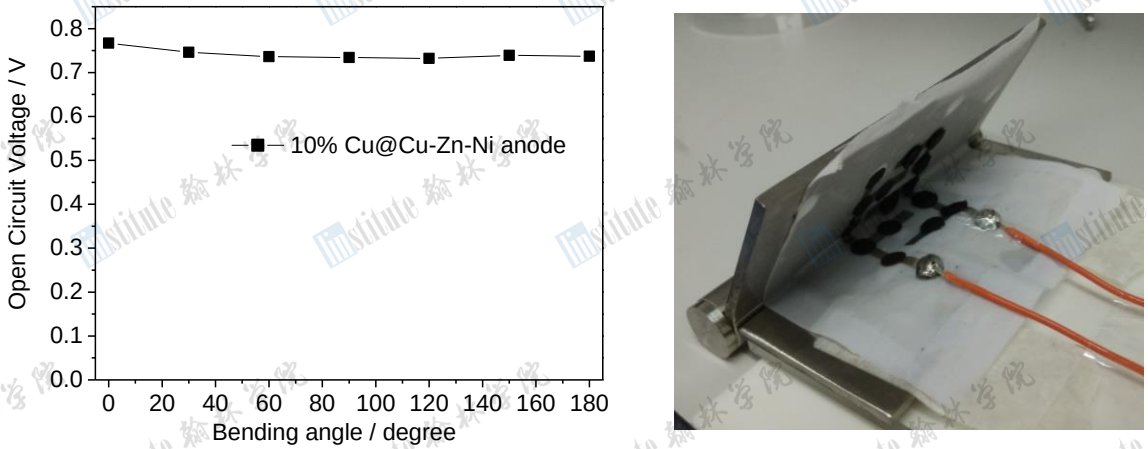

Figure 6.2 DUFC output voltage at different bending angle

6.2.2 Effect of flexible substrate for DUFC

In order to prepare an efficient wearable DUFC using sweat as fuel, a suitable bendable substrate should be used for absorbing and keeping sweat during an exercise. It is expected that the duration of power generated depends on the availability of sweat. Two flexible, commercially available solid substrates, polyester fabric and hydrogel film, were used to prepare two prototypes and were adhered on the skin (front arm, chest and shoulder blade) of the experimenter. The DUFC using hydrogel film demonstrated a much better performance than that of using polyester textile as substrate and it can be rationalized from the relative ability of sweat retention in polyester textile and hydrogel (Figures 6.3). A hydrogel is composed of a network of hydrophilic polymer chains that have high affinity towards water (or sweat). More fuel (sweat) in the DUFC leads to a more stable and long-lasting performance.

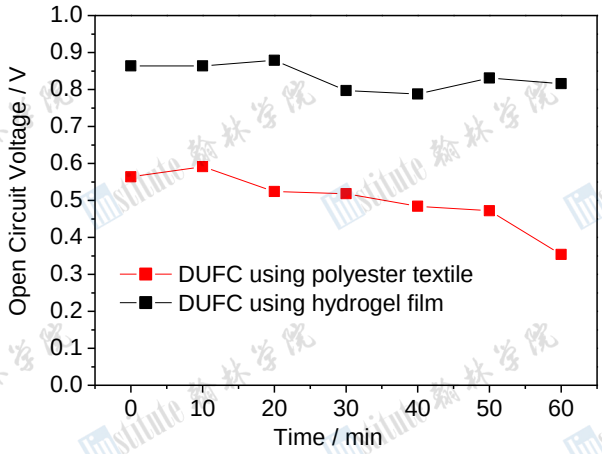

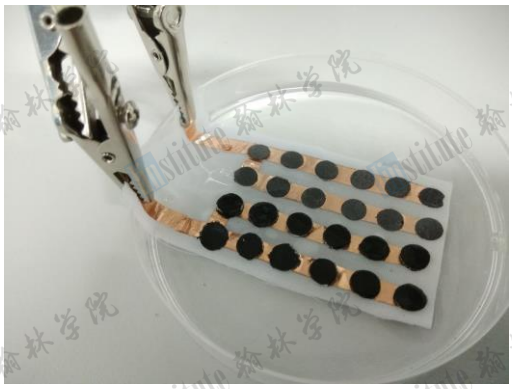

Figure 6.3

(a) Top left: Output voltage of DUFC using different substrate

(b) Top right: DUFC using polyester textile as substrate

(c) Bottom left: DUFC using hydrogel film as substrate

6.2.3 Effect of muscle movement and position of body

From the practical point of view, wearable DUFC is an energy harvesting device using sweat as the fuel to power on electrical applicant or sensor used to monitor the human physiological parameter during exercise. The performance of wearable DUFC may be governed by the amount and rate of sweat secretion, and level of muscle movement. Hence, three positions (front arm, chest and shoulder blade) were chosen to test the performance of our prototype DUFC. The reasons of choosing these three areas are (1) rate and amount of sweat secretion and (2) presence of flat surface of skin. Moreover, the DUFC was tested under different body posture or movement including muscle contraction/relaxation, chest expansion/relaxation and under pressure (Figures 6.4). Figure 6.5 summarize the peak voltage recorded in different position and situation. Output voltages of DUFC were kept fairly constant at 0.73 V to 0.79 V wherever the position and condition of measurement. Somehow the measured value increases with the degree of DUFC compression on skin. Higher output voltage was recorded under muscle contraction or chest expansion, and the reading was even higher under pressure.

Figures 6.4 (a) From Left to Right: Upper front arm under muscle relaxation, contraction and pressure

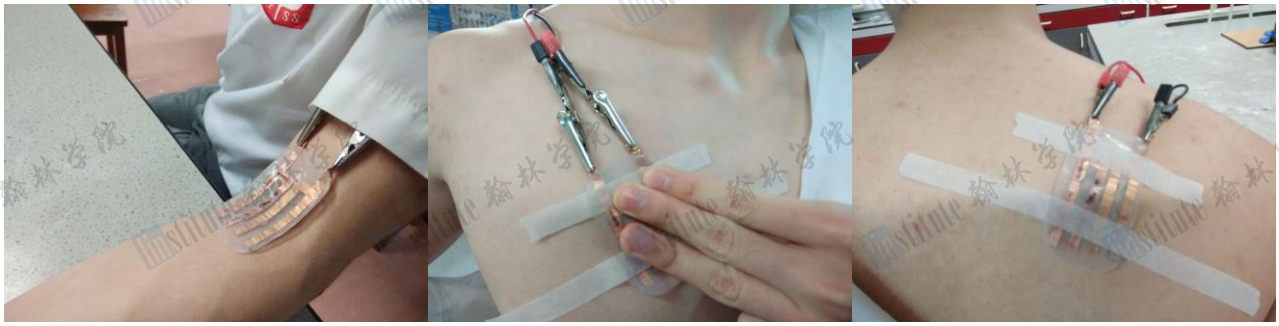

Figures 6.4 (b) From Left to Right: near the joint, on the chest and shoulder blade

Position	Upper Front arm			Chest			Shoulder blade
Condition	Relaxing	Contracting	Forcing	Relaxing	Expanding	Forcing	Relaxing
Peak voltage, V	0.731	0.741	0.791	0.754	0.796	0.793	0.770

Figures 6.5 Summary of the peak voltage measured in different body position and condition

6.2.3 Using human sweat as the fuel for DUFC

Finally, the prototype DUFC (10% Ni-doped Cu@Cu-Zn as anode, C/CQD as cathode and hydrogel as flexible substrate) was fixed on the sweat belt with the layer of gauze to prevent direct contact of electrode discs and skin. Experimenter wore the sweat belt and performed 15 minutes exercise, to get sweaty, and the performance of DUFC was measured when experimenter was at rest (Figure 6.6). The DUFC demonstrated a promising performance with the output power density of 12.1 mW cm^{-2} and energy capacity of 15 mWh. The performance can be further enhanced by increasing the size of DUFC or connecting several DUFC in series, so as to further boost the performance of DUFC (Figure 6.7).

Figure 6.6 (a) Left: DUFC using 10% Ni-doped Cu@Cu-Zn as anode, C/CQD as cathode and hydrogel as flexible substrate

(b) Middle: A piece of gauze covers the side with electrode discs of DUFC, and DUFC is fixed on the sweat belt.

(c) Right: Experimenter wearing the sweat belt with DUFC

Parameter	V_{OC}	Capacity	Energy capacity	Power density
Prototype	0.720 V	34 mAh	15 mWh	12.1 mW cm^{-2}

Figure 6.7 Performance of DUFC using sweat as the fuel, after 15 minutes physical exercise

Section VII Conclusion

In this project, the optimum intrinsic (anodic and cathodic catalyst) and extrinsic parameters (effect of temperature, concentration of fuel, type of substrate) of DUFC have been extensively investigated. During this research, several challenging problems needed to be addressed. These include synthesizing the nanostructure of Ni-doped Cu-Zn alloy on Cu foam; carbon quantum dots from gelatin; and enhancing the electrochemical performance by optimizing working pH, temperature and concentration of anodic electrolyte and fabricating the wearable DUFC testing prototype.

The effect of anodic catalyst (Ni-doped Cu@Cu-Zn nanostructures loading) and their corresponding working pH environment towards the overall performance of DUFC were studied. Generally, the performance of DUFC is pH-dependent and output power density increase with increasing pH, showing 83% increases from pH 1.0 to 13.0. The electrode is chemically stable and is able to performance steady in extreme pH. Similarly, our DUFC is functionable over a wide range of temperature and at lower concentration of urea. It is particularly important for DUFC perform normally at low concentration of urea as the urea amount in sweat is in the range of 20 mM to 40 mM.

Various types of anode were prepared to study the effect of materials, nanostructure and Ni-doping. It shown that Cu@Cu-Zn shows a catalytic property toward the oxidation of urea, exhibiting almost 3 times higher in power density of Cu@Cu electrode, while further 16% enhancement was contributed by the nanostructure of Cu-Zn on Cu foam. The extraordinary performance can be rationalized from the presence of nanostructure of either Cu or Cu-Zn and their orderly alignment of nanostructure on the copper foam providing hierarchical structure with both macropores and mesopores with extensive resistance-free pathway, which facilitate the diffusion of ions or molecules between electrode and diffusion layer of solution film, and large surface area-to-volume ratio for redox reactions.

Another 18% increment was contributed by 8% Ni doping on Cu@Cu-Zn anode. Effect of Ni-doping was further investigated by varying the percentage of Ni-doping from 0 to 20%. The maximum power density of 15.16 mW cm^{-2} was found if there are 10% of Ni-doping. Its performance climbs drastically from 0% to 10% Ni-doping, and then levels off. Such effect can be rationalized from the high disorder structure of Cu-Zn lattice that provide more catalytic site for the oxidation of urea.

CQDs was synthesized from the carbonization of gelatin by hydrothermal method. The aim of this process is to prepare the carbon-based catalyst in nanoscale to catalyst the cathodic oxygen reduction reaction. The identity of the as-synthesized sample was examined and confirmed by fluorescent analysis. All samples show the distinguished PL peak from 450 nm to 600 nm, with the peak maximum at 500 nm. It is found that the blue photoluminescence of CQD loss if the temperature or duration of hydrothermal treatment increases. This dramatic change can be rationalized from the increasing size of CQD under the prolonged hydrothermal treatment at higher temperature.

From the results of DUFC performance test, DUFC using CQD as cathodic catalyst show close relationships to the natural of catalysts loaded on anode and cathode. Our DUFC can be greatly improved by applying nanotechnology technique on the carbon-based catalyst synthesis. The maximum cell performance was achieved for a C/Pt air cathode and C/CQD air cathode with peak power 15.16 mW cm^{-2} and 14.26 mW cm^{-2} at current density of 32 mA cm^{-2} respectively. Although the performance of DUFC using C/CQD air cathode is not as good as the one of using C/Pt cathode, using carbon-based CQD as the catalyst in cathode already opens up the possibility of development of green DUFC for new generation.

Lastly, four practical trials were performed to check the feasibility of using sweat as fuel, effect of bendability and its performance on different part of body and posture. Our model shows a stable output voltage throughout the wide range of bending angle from 0^{o} to 180^{o}, which means that our model is suitable to be worn near the joint position or any part of body with relatively large movement. Secondly, the model exhibits a steady performance on different parts of body (front arm, chest and shoulder blade) and condition (muscle contraction / relaxation, check expansion / relaxation). It is noted that the amount of sweat required to initiate the DUFC is very small. As the duration of power generated depends on the availability of sweat, 2 commercially available flexible substrates, polyester fabric and hydrogel film were used. Hydrogel film is an ideal material for wearable DUFC as it has high sweat-retention ability to hold the fuel (sweat). Finally, one wearable DUFC can give a promising performance with the output power density of 12.1 mW cm^{-2}, energy capacity of 15 mWh and peak voltage of 0.720 V after 15 minutes physical exercise.

In conclusion, the wearable DUFC has been developed with promising electrochemical performance. The nano-architecture of both anodic and cathodic catalyst enables efficient charge transport, electrode stability

and catalytic activity, allowing the DUFC with high power density (15.2 mW cm^{-2} under current density of 30.6 mA cm^{-2}), high capacity of 47 mAh and energy capacity of 20 mWh, which open up the possibility of developing the real-life application of a soft, flexible wearable direct urea fuel cell.

Appendix

Reference

1. Sue, C. Y. & Tsai, N. C. *Appl. Energy*. **2012**, 93, 390–403.
2. Shaikh, F. K. & Zeadally, S. *Renew. Sustain. Energy Rev.***2016**, 55 1041–1054.
3. Khaligh, A., Zeng, P. & Zheng, C. *IEEE Trans. Ind. Electron.* **2010,** 57, 850–860.
4. Xu, S. et al. *Nat. Nanotechnol.* **2010**, 5, 366–373.
5. Bourzac, K. *C&EN,* **2019***,* 97, 6–6.
6. Kim, J., Jeerapan, I., Sempionatto, J. R., Barfidokht, A., Mishra, R. K., Campbell, A. S., Hubble, L. J., Wang, J. *Acc. Chem. Res.* **2018**, 51, 2820–2828.
7. Ray, T. R., Choi, J., Bandodkar, A. J., Krishnan, S., Gutruf. P., Tian, L., Ghaffari, R., Rogers, J. A. *Chem. Rev.* **2019**, 119, 5461–5533.
8. Bandodkar, A. J., You, J. M., Kim, N. H., Gu, Y., Kumar, R., Mohan, A. M. V., Kurniawan, J., Imani, S., Nakagawa, T., Parish, B., *Energy Environ. Sci.* **2017**, 10, 1581−1589.
9. Lan, R., Tao, S., Irvine, J. T. S. *Energy Environ. Sci***. 2010**, 3, 438-441.
10. Barakat, N. A. M., Algiami, M., Ghouri, Z. K., Al-Meer, S. *Int. J. Electrochem. Sci*. **2018**, 13, 4693 – 4699.
11. Barakat, N. A. M., Algiami, M., Obaid, M., Al-Meer, S. *Catal. Commun.* **2017**, 97, 32 – 36.
12. Zeng, M., Wu, J., Li, Z., Wu, H., Wang, J., Wang, H., He, L., Yang, X. *ACS Sustainable Chem. Eng*. **2019**, 7, 4777 – 4783.
13. Lee, Y. W., Kim, B. S., Hong, J., Lee, J., Pak, S., Jang, S. P., Jang, H. S., Whang, D., Cha, S. N., Sohn, J. I., Kim, J. M. *J. Mater. Chem. A*, **2016**, 4, 10084 – 10090.